

# Charge and spin-currents in current-perpendicular-to-plane nanoconstricted spin-valves

N. Strelkov<sup>1,2</sup>, A. Vedyayev<sup>1,2</sup>, N. Ryzhanova<sup>1,2</sup>, D. Gusakova<sup>1,3,a</sup>, L. D. Buda-Prejbeanu<sup>1,4</sup>, M. Chshiev<sup>1</sup>, S. Amara<sup>1</sup>, N. de Mestier<sup>1</sup>, C. Baraduc<sup>1</sup>, B. Dieny<sup>1</sup>

<sup>1</sup>*SPINTEC (UMR8191 CEA/CNRS/UJF/G-INP), CEA Grenoble, INAC, 38054 Grenoble Cedex 9, France*

<sup>2</sup>*Lomonosov University, Faculty of Physics, Department of Magnetism, Moscow, Russia*

<sup>3</sup>*CEA-LETI, MINATEC, DRT/LETI/DIHS, 38054 Grenoble Cedex 9, France*

<sup>4</sup>*Grenoble InP, 46, avenue Félix Viallet, 38031 Grenoble Cedex 1 France*

## ABSTRACT

The charge and spin diffusion equations taking into account spin-flip and spin-transfer torque were numerically solved using a finite element method in complex non-collinear geometry. As an illustration, spin-dependent transport through a non-magnetic nanoconstriction separating two magnetic layers was investigated. Unexpected results such as vortices of spin-currents in the vicinity of the nanoconstriction were obtained. The angular variations of magnetoresistance and spin-transfer torque are strongly affected by the structure geometry.

**Keywords:** spin polarized transport, spin transfer torque

**PACS numbers:** 72.25.-b, 75.70.Cn, 85.75.-d

<sup>a</sup>Electronic mail: [daria.gusakova@cea.fr](mailto:daria.gusakova@cea.fr)

Since the discovery of Giant Magnetoresistance (GMR) in 1988<sup>1</sup>, the field of spin electronics has steadily expanded, stimulated by both fundamental breakthrough discoveries (tunnel magnetoresistance (TMR) at room temperature<sup>2,3</sup>, spin transfer torque<sup>4,5</sup> (STT), voltage controlled magnetic devices<sup>6</sup>) and a strong synergy between basic research and industrial developments (magnetoresistive heads for hard disk drives<sup>7</sup>, Magnetic Random Access Memories (MRAM)<sup>8</sup>, logic devices<sup>9</sup>, RF oscillators<sup>10</sup>). In the same time the scientific community profited by the advances in theoretical research such as interpretation of GMR in terms of spin-dependent scattering<sup>1,7,11</sup> or prediction of STT as a result of exchange interaction between spin polarized conduction electrons and those responsible for the local magnetization<sup>4,5</sup>. The introduction of the spin-accumulation and spin-diffusion length concepts to describe the diffusive transport in current-perpendicular-to-plane (CPP) metallic multilayers<sup>12</sup> and its generalization to non-collinear magnetic configurations is of particular importance<sup>13-16</sup>. However, this fundamental knowledge has been applied so far only for very simple geometries with homogeneous current flow. In contrast, most spintronic devices under research or development such as point contacts<sup>17,18</sup>, low resistance tunnel junctions with current crowding effects<sup>19</sup>, GMR CPP magnetoresistive heads and current confined path (CCP) structures<sup>20,21</sup> involve inhomogeneous current flows.

The purpose of the present numerical study was to investigate the peculiar effects which may arise in spin-dependent transport when the charge current flow is highly non-uniform for geometrical reasons. We illustrate that unexpected phenomena such as vortices of spin-current can appear as a result of the system geometry and associated current non-uniformity. Such phenomena can strongly influence the magnetization dynamics and must be properly taken into account for spintronic devices design.

The formalism we use here was proposed by Zhang *et al*<sup>13</sup> and is based on generalization of the Valet and Fert theory<sup>12</sup> in the diffusive limit. Each material constituting the system of

arbitrary shape and composition is described by local transport parameters ( $C_0$ –conductivity,  $\beta$ –spin asymmetry of  $C_0$ ,  $D_0$ –diffusion constant related to  $C_0$  via Einstein relation<sup>13</sup>,  $\beta'$ –spin asymmetry of  $D_0$ ,  $N_0$ –density of state at Fermi level). Interfacial scattering is usually described by introducing thin layers (of typical thickness of 0.3nm) having bulk parameters corresponding to the interfacial ones<sup>12,22</sup>.

For this study we assume  $\beta=\beta'$  in the following and omit the interfacial scattering. All transport properties are then described by 4 local variables: the scalar electrostatic potential  $\tilde{\varphi}$  and the 3 components of spin accumulation in spin-space ( $m_x, m_y, m_z$ ). The local normalized charge current vector is then given by:

$$\mathbf{j}^e = \frac{2C_0}{e} \nabla \tilde{\varphi} - \frac{2\beta C_0}{e^2 N_0} (\mathbf{u}_M, \nabla \mathbf{m}) \quad (1),$$

and the normalized spin current is described by a tensor with 3 coordinates for both spin and real space as:

$$\mathbf{j}^m = \frac{2\beta C_0}{e} \mathbf{u}_M \nabla \tilde{\varphi} - \frac{2C_0}{e^2 N_0} \nabla \mathbf{m} \quad (2).$$

where  $\mathbf{u}_M$  and  $e$  represent a unit vector parallel to the local magnetization and electron charge, respectively.

The 4 variables are then calculated in steady state everywhere in space by solving the set of fundamental equations of spin-dependent diffuse transport:

$$\left\{ \begin{array}{l} \operatorname{div} \mathbf{j}^e = 0 \\ \operatorname{div} \mathbf{j}^m + \frac{J_{sd} V M_s}{\hbar \mu_B} (\mathbf{m} \times \mathbf{u}_M) + \frac{\mathbf{m}}{\tau_{sf}} = 0 \end{array} \right. \quad (3),$$

$$\left\{ \begin{array}{l} \operatorname{div} \mathbf{j}^e = 0 \\ \operatorname{div} \mathbf{j}^m + \frac{J_{sd} V M_s}{\hbar \mu_B} (\mathbf{m} \times \mathbf{u}_M) + \frac{\mathbf{m}}{\tau_{sf}} = 0 \end{array} \right. \quad (4),$$

where  $J_{sd}$ ,  $M_s$ ,  $V$  and  $\tau_{sf}$  represent *s-d* exchange interaction constant, saturation magnetization, volume and spin relaxation time, respectively;  $\hbar$  and  $\mu_B$  are Planck constant and Bohr magneton. The Eq. (3) expresses the conservation of charge while Eq. (4) states that the spin polarization of the current is not conserved. It can vary either due to spin relaxation

or local spin-transfer torque given by  $\mathbf{T} = \frac{J_{sd} VM_S}{\mu_B} (\mathbf{m} \times \mathbf{u}_M)$ . The constant  $J_{sd}$  and time  $\tau_{sf}$  are related to spin-reorientation length  $\lambda_J = \sqrt{2\hbar D_0 / J_{sd}}$  and spin-diffusion length  $l_{sf} = \sqrt{2(1 - \beta^2) D_0 \tau_{sf}}$ .

Using this general formalism, the spin-dependent transport was investigated in two dimensional nanoconstricted spin-valve represented in Fig. 1. It consists of two 3nm thick magnetic layers ( $M_1, M_2$ ) separated by a non-magnetic metallic nanoconstriction 2nm long and varying width. This central magnetic system is sandwiched between two thick non-magnetic metallic electrodes. We assume that somehow, the relative orientation of the magnetizations in the two magnetic layers can be varied in-plane. At outer boundaries, we impose no perpendicular component of charge and spin current except at the boundaries where a potential is applied. Voltages of  $\varphi_{in} = 0V$  ( $\varphi_{out} = 50mV$ ) are uniformly applied on the left (right) surface of the left (right) electrode, respectively.

Using a finite element technique, we solved the system of equations 1–4 and obtained the spatial distribution of the spin accumulation and charge current vectors, spin-current tensor, in-plane and perpendicular components of spin-transfer torque as a function of the angle between the magnetizations of the two layers.

We used the following bulk parameters to represent materials comprising the system<sup>23</sup>:  $C_0 = 0.005\Omega^{-1}\text{nm}^{-1}$ ,  $\beta = 0.6$ ,  $l_{sf} = 20\text{nm}$  for magnetic layers and  $C_0 = 0.02\Omega^{-1}\text{nm}^{-1}$ ,  $l_{sf} = 50\text{nm}$  for outer electrodes and nanoconstriction. Under these assumptions, the resistance of the stack per 1nm of depth in parallel (antiparallel) configuration is  $R_P = 209\Omega$  ( $R_{AP} = 210\Omega$ ), yielding a magnetoresistance  $\Delta R/R_P = 0.5\%$ .

Fig.2 shows the charge current and electrostatic potential distribution throughout the structure in antiparallel magnetic configuration. As expected, the current converges towards the constriction creating a significant component along magnetization within the magnetic

layer and diverges afterwards while the voltage gradient reaches maximum across the constriction.

Fig. 3 shows the spin-current distribution of the component parallel to the  $y$ -axis, i.e. to the magnetization of the reference layer (the layer on the left of the constriction), and corresponding spin accumulation component. As one can see in the parallel configuration (Fig.3(a)), the spin current looks very similar to the charge one (see Fig. 2). It gradually increases its amplitude towards the constriction due to the increment of both current polarization (over a length scale  $l_{sf}$ ) and charge current density. A symmetric decrease occurs on the other side of the constriction. The spin accumulation is zero in the middle of the constriction with an excess of spins antiparallel to magnetization on the left (since the electrons with opposite spin direction more easily traverse the reference layer) and an excess of spins parallel to magnetization on the right. At  $90^\circ$  configuration (Fig.3(b)), spin current amplitude very rapidly drops to zero when the electrons tend to penetrate to the right magnetic layer. This decay takes place over the length scale  $\lambda_s$  ( $\sim 1\text{nm}$ ) much shorter than  $l_{sf}$  ( $\sim 20\text{nm}$ ) involving much steeper gradient of spin current amplitude on the right hand side of constriction Fig.3(b). Finally, the situation of antiparallel configuration (Fig.3(c)) is particularly interesting because it unexpectedly reveals the formation of spin current vortices on both sides of the constriction. Indeed, a significant component of charge current collinear to magnetization flowing over a long distance within the magnetic layers is responsible for the high polarization of spin current (in positive  $y$ -direction on the left side and negative on the right side). On left side converging electron current brings the spins aligned with positive  $y$ -axes towards the constriction and on the right side it takes away the spins aligned with negative  $y$ -axes. Thus in total a large flow of spins aligned with positive  $y$ -axis converges towards the constriction along the interfaces from both sides. In same time due to the fact that the spin accumulation is very large in the constriction and rapidly vanishes away from it in the

direction perpendicular to the interfaces, it generates the diverging y-component of spin current along the same direction. The combination of these two phenomena gives raise to vortices of spin current on both sides of the constriction.

We also compute the dependence of the CPP resistance of the structure as a function of angle  $\theta$  between the magnetizations of ferromagnetic layers (Fig.4). Fig.4 actually compares the CPP-R( $\theta$ ) in presence of the 5nm wide constriction and without constriction (i.e. constriction replaced by a continuous Cu spacer). The presence of the constriction clearly affects the shape of the CPP-R( $\theta$ ) variation. Interestingly both variations can be very well fitted with the expression proposed by Slonczewski<sup>24</sup>:  $r = (1 - \cos^2 \theta / 2)(1 + \chi \cos^2 \theta / 2)^{-1}$ , where  $r$  is the reduced resistance defined by  $r = (R(\theta) - R(0))(R(\pi) - R(0))^{-1}$ . However, the  $\chi$  values in the above expression are quite different in the two situations i.e.  $\chi=15.86$  and  $4.24$  respectively for the continuous spacer and nanoconstricted spacer. This result points out that the device geometry can strongly impact the angular variation of CPP-GMR, an effect certainly important to take into account in the design of CPP-GMR devices, particularly GMR heads for hard disk drives.

As a further step, we calculated the spin transfer torque exerted by the spin polarized current on the right magnetic layer as a function of the angle between the two magnetizations (Fig.5). In the general case, the torque has two components: a component in the plane formed by the magnetizations of the two magnetic layers (sometimes called Slonczewski's term<sup>4</sup>) and a component perpendicular to it (also called field-like term<sup>13</sup>). In metallic CPP spin-valves, it is generally argued that the field like term is weak as a result of averaging over all incidences of conduction electrons penetrating in the ferromagnetic layer.

Fig.5 (a) and (b) show the angular variation of the two components of spin-torque integrated over the whole volume of the free layer assuming various sizes of the constriction (no constriction or constriction diameter equals to 2 or 5nm). Our results confirm that in this

diffusive approach, the perpendicular component of spin-torque is two orders of magnitude smaller than the in-plane torque. It is interesting to note that the shape of the angular variation of spin transfer torque is quite similar for the two components. Actually, these shapes can also be very well described by the expression proposed by Slonczewski for the reduced torque<sup>24</sup>:

$$\tau(\theta) = \sin \theta (\Lambda \cos^2(\theta/2) + \Lambda^{-1} \sin^2(\theta/2))^{-1}$$

both for the in-plane and perpendicular components. However, as for the angular variation of GMR, the  $\Lambda$  fitting parameter strongly depends on the size of the constriction ( $\Lambda$  respectively equals to 4.09, 2.19, 1.75 for no constriction, constriction with diameter 5nm and 2nm). Note that the equality<sup>24</sup>  $\Lambda^2 = \chi + 1$  is verified quite well for the case without constriction and laterally homogenous electron current. Fig.5(c) shows a map of the in-plane spin-transfer torque amplitude for 90° magnetic orientation in the case of the 10nm wide constriction. Clearly, the spin transfer torque is most important in the immediate vicinity of the constriction where the current density is the largest. Actually the gradient of spin transfer torque is quite large since the charge current density drops very quickly around the edges of the constriction. That points out that new length scales may emerge in these confined geometries due to a balance between spin-torque gradient and exchange stiffness. In micromagnetic simulations, traditionally only two length scales are considered: the Bloch wall width (balance between anisotropy and exchange stiffness) and exchange length (balance between magnetostatic energy and exchange stiffness). It is likely that additional length scales will have to be considered in structures with strong current gradient.

In conclusion, a numerical approach has been developed to compute the charge and spin-current in magnetic structures of arbitrary shape and composition. The case of nanoconstricted spin-valves was treated as an illustration. Charge and spin-current clearly behave very differently as demonstrated for instance by the formation of spin current vortices. This type of tool should be most helpful in the design of functional spintronic devices as well as for the

quantitative interpretation of experimental data in devices with non uniform or non-local currents such as lateral spin-valves<sup>25</sup>.

This project has been supported in parts by the European RTN “Spinswitch” MRTN-CT-2006-035327 and partially by Chair of Excellence Program of the Nanosciences Foundation (Grenoble, France).

## REFERENCES

<sup>1</sup> M. Baibich *et al*, Phys.Rev.Lett. **61** 2472 (1988); G. Binasch, P. Grunberg, F. Saurenbach, W. Zinn, Phys. Rev. B 39. 4828 (1989).

<sup>2</sup> J. S. Moodera, L. R. Kinder, T. M. Wong, R. Meservey, Phys.Rev.Lett **74** , 3273 (1995).

<sup>3</sup> T. Miazaky, N. Tezuka, Journ. Magn. Magn. Mater. **139**, L231 (1995).

<sup>4</sup> J. C. Slonczewski, Journ. Magn. Magn. Mater. **159**, L1 (1996).

<sup>5</sup> L. Berger, Phys. Rev. B **54**, 9353 (1996).

<sup>6</sup> H. Ohno *et al*, Nature **408**, 944 (2000).

<sup>7</sup> B. Dieny *et al*, Phys. Rev. B **43**, 1297 (1991); A. Vedyayev *et al*, JMMM **172**, 53 (1997).

<sup>8</sup> M. Durlam *et al*, IEEE Journ. Solid State Circuits **38**, 769 (2003).

<sup>9</sup> S. Matsunaga *et al*, Appl. Phys. Express **1**, 091301 (2008).

<sup>10</sup> D. Houssameddine *et al*, Nature Materials **6**, 447 (2007).

<sup>11</sup> W. P. Pratt, Phys. Rev. Lett. **66**, 3060 (1991).

<sup>12</sup> T. Valet, A. Fert, Phys. Rev. B **48**, 7099 (1993).

<sup>13</sup> S. Zhang, P. M. Levy, A. Fert, Phys. Rev. Lett. **88**, 236601 (2002).

<sup>14</sup> M. D. Stiles, A. Zangwill, J. Appl. Phys. **91**, 6812 (2002).

<sup>15</sup> M. D. Stiles and A. Zangwill, Phys. Rev. B **66**, 014407 (2002).

<sup>16</sup> A. Shapiro, P. M. Levy, S. Zhang, Phys. Rev. B **67**, 104430 (2003).

<sup>17</sup> S. Kaka *et al*, Nat. Lett. **437**, 389 (2005).

<sup>18</sup> F. B. Mancoff *et al*, Nat. Lett. **437**, 393 (2005).

<sup>19</sup> J. Chen *et al*, Journ. Appl. Phys. **91**, 8783 (2002).

<sup>20</sup> K. Nagasaka *et al*, Journ. Appl. Phys. **89**, 6943 (2001).

<sup>21</sup> H. Fukazawa *et al*, IEEE Trans. Mag. **40**, 2236 (2004).

<sup>22</sup> W. Park *et al*, Phys. Rev. B **62**, 1178 (2000).

<sup>23</sup> A. Fert, L. Piraux, Journ. Magn. Magn. Mater. **200**, 338 (1999).

<sup>24</sup> J. C. Slonczewski, Journ. Magn. Magn. Mater. **247**, 324 (2002).

<sup>25</sup> T. Kimura *et al*, J. Phys.: Condens. Matter **19**, 165216 (2007).

## FIGURES CAPTIONS

FIG. 1. (color online) Scheme of nanoconstricted spin-valve.

FIG. 2. (color online) Zoom around the nanoconstriction showing the charge current flow through the constriction corresponding to the antiparallel state (arrows) and electrostatic potential (color mapping).

FIG. 3. (color online) Zoom around the nanoconstriction:  $y$ -component of spin current (black arrows) and  $y$ -component of spin accumulation (color mapping) for three magnetic configurations: (a) parallel, (b)  $90^\circ$ , (c) antiparallel. In Fig.3(c), the white arrows remind the charge flow and the grey closed arrows indicate the formation of spin current vortices which are better evidenced in the inset.

FIG. 4. Angular variation of the CPP reduced resistance with and without constriction. The dots are the calculated values and the lines are fits according to Slonczewski's expression (see text).

FIG. 5. (color online) (a) In-plane and (b) perpendicular components of averaged spin-transfer torque over the whole volume of the “free” (right) magnetic layer as a function of the angle between the magnetizations. (c) Mapping of the amplitude of the in-plane torque for  $90^\circ$  magnetic configuration in the presence of the 10nm wide constriction.

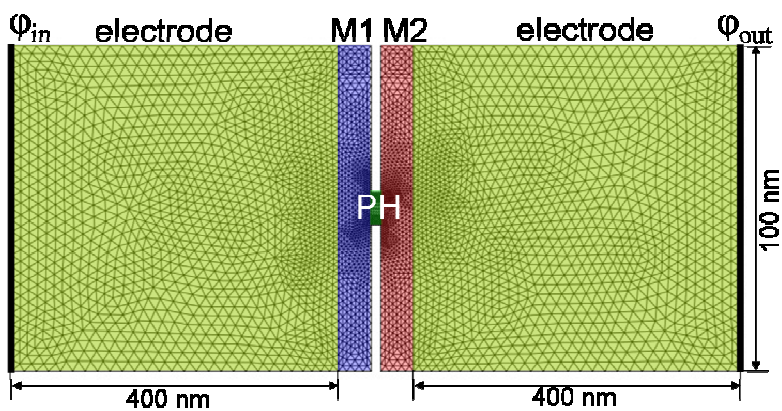


FIG. 1.

N. Strelkov *et al*

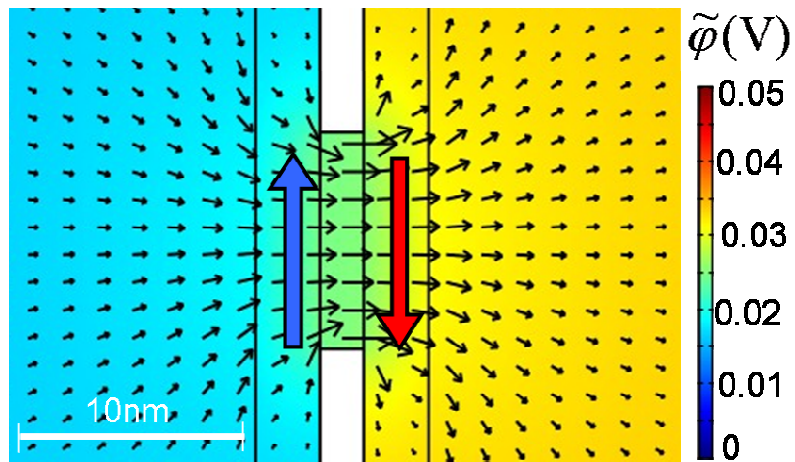


FIG. 2.

N. Strelkov *et al*

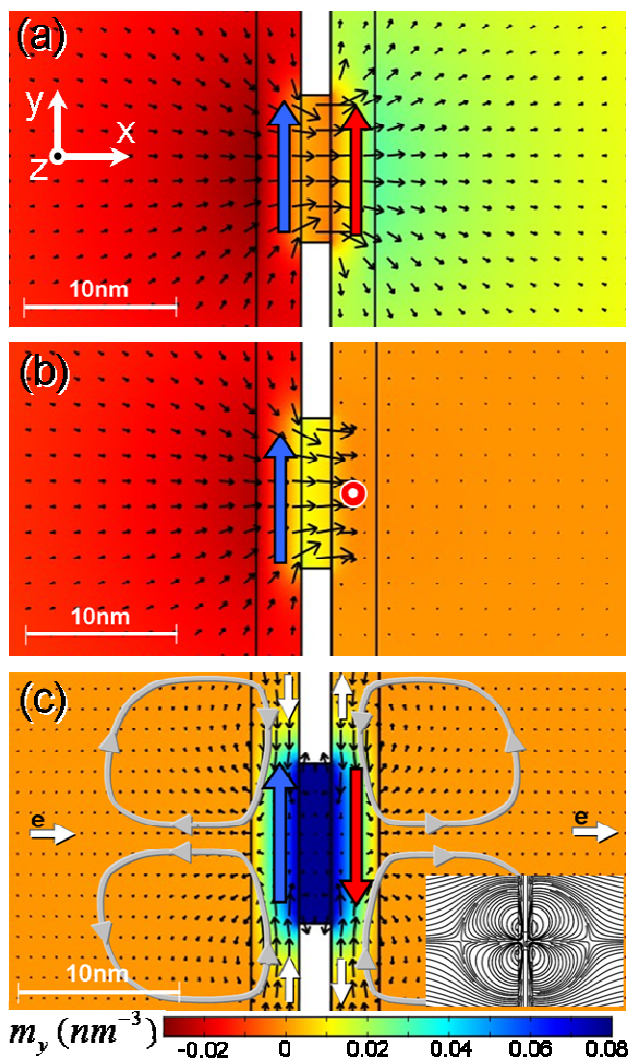


FIG. 3.

N. Strelkov *et al*

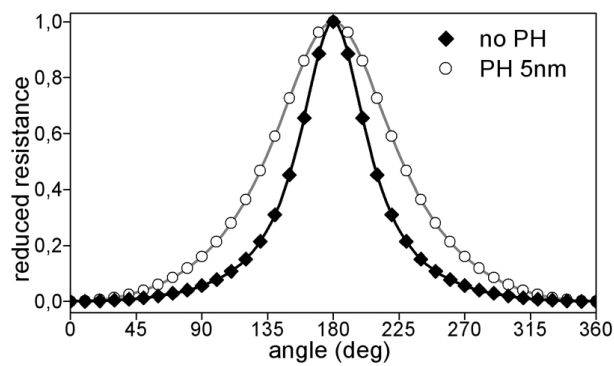


FIG. 4.

N. Strelkov *et al*

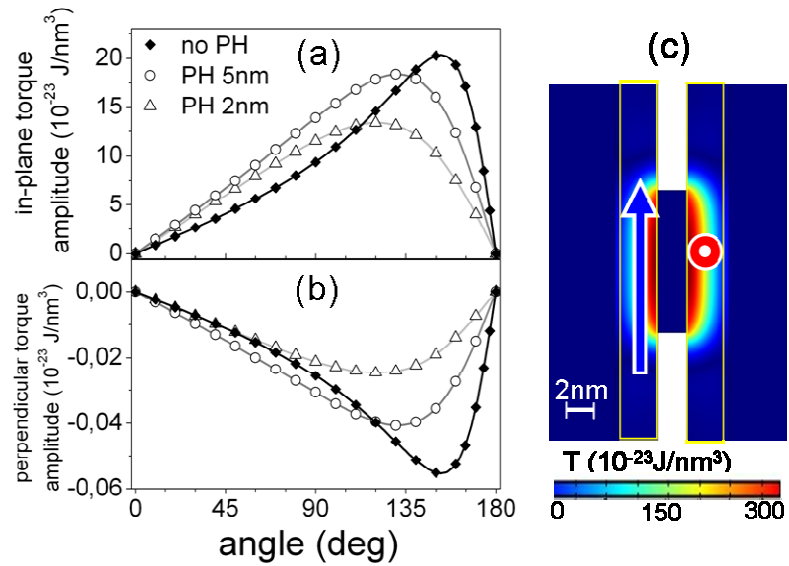


FIG. 5.

N. Strelkov *et al*